

# Design and Control of Standalone DC Fast Charging Station Based on Photovoltaic and Battery Energy Storage, Case Study: Alamein Egypt

Mohamed Selmy<sup>1</sup>, Ahmed Nabil<sup>\*1</sup>, H. A. Mansour<sup>1</sup> and Ahmed M. Hussein<sup>1</sup>

<sup>1</sup>Department of Electrical Power Engineering, Faculty of Engineering at Shoubra, Benha University, Cairo, Egypt

\* Corresponding Author.

E-mail: drhassan.mansour@yahoo.com , ahmednabil\_1995@yahoo.com, mohamed.selmy@feng.bu.edu.eg  
ahmed.hussein@feng.bu.edu.eg

**Abstract:** The world is moving toward reliance on electric vehicles as a substitute for internal combustion engine vehicles due to global concerns about climate change. The main barriers to the widespread adoption of electric vehicles are long charging times and lack of infrastructure. Fast charging stations can solve these problems, but fast charging stations present a large and unexpected load on the grid. One of the solutions to mitigate the impact of fast charging stations on the grid is to use renewable energy sources and energy storage. This paper proposes the design and control of a 100 kW standalone DC fast charging station with two charging slots based on photovoltaic power and battery energy storage. The station location is in Alamein, Egypt. Station sizing is carried out based on a real load profile using HOMER software. MATLAB Simulink is used to verify station performance under real weather conditions and solar irradiance of the station location. The results show that the proposed station can meet various load conditions.

**Keywords:** Standalone Fast Charging Station, Photovoltaic (PV), Electric vehicles, Parallel Resonant Converter

## 1. INTRODUCTION

The transportation sector is one of the most significant contributors to greenhouse gas emissions. These emissions have negative effects on the environment and human health [1]- [3]. The world is moving toward reliance on electric vehicles (EVs) as an alternative to internal combustion engine vehicles.

The main obstacles to electric vehicles' widespread adoption are high cost, long charging times, battery lifetime, lower driving range, and lack of infrastructure. Fast charging stations (FCS) can be used to reduce EV charging time.

FCS feeds directly from the grid, presenting a large load on the grid. The FCS load may require electric service upgrading [4], [5]. Also, it influences the power quality of the grid. The issues of power quality include harmonic current distortion, voltage unbalance, voltage fluctuation, etc. [6]-[7].

One of the solutions to mitigate the impact of FCS on the grid is to integrate energy storage (ES) such as batteries, flywheels, and hydrogen with the grid. The energy storage can store power during light loads on the grid and deliver it

during peak loads which can save on the cost of electric service upgrades [8]- [10].

There is another solution represented in using renewable energy sources (RES) such as solar, biomass, and wind as sources of energy in EV charging stations. The main issue with RES is their uncertain nature [11]. Using hybrid RES or RES with energy storage can mitigate this problem.

EV charging stations can be classified into main five categories [12], [13], as follows: (1) standalone charging station based on RES, (2) standalone charging station based on RES and ES, (3) hybrid charging station based on grid and ES, (4) hybrid charging station based on grid and RESs, and (5) hybrid charging station based on grid, RESs, and ES.

A charging station powered by photovoltaic (PV) energy is presented in [14]. However, the authors do not take into consideration that solar radiation is very low on a rainy day, resulting in very low energy production. The low energy production may affect the system's reliability. In [15], a hybrid charging station in Turkey based on PV and wind energy is designed based on HOMER software. A

standalone charging station based on PV and battery energy storage is discussed in [16], but the power of PV and battery energy storage is very low, which is not suitable for fast charging station requirements. A mathematical model and control of a charging station based on the grid and battery energy storage is presented in [17]. In [18], an energy management strategy to coordinate the exchange of power between the grid and PV is discussed. An optimization model for an EV charging station based on the grid, PV, and battery is presented in [19].

EV charging station architecture can be either an AC bus configuration, a DC bus configuration, or a DC and AC configuration. Power electronic converters are important elements at various types of EV charging stations. These converters can be AC/DC, DC/AC, or DC/DC. The DC/DC converter can be unidirectional or bidirectional. Also, The DC/DC converter can be isolated or non-isolated. The boost converter is the most common unidirectional non-isolated DC/DC converter used between PV and the DC bus as in [20]. In [21], a flyback converter which is unidirectional isolated DC/DC is used between PV and the DC bus. For safety reasons, the isolated DC/DC converter unidirectional or bidirectional shall be used with EVs. Non-isolated bidirectional DC/DC converters are used with energy storage devices such as buck-boost converter or T-source converter as in [22]. The AC/DC converters can be used with the grid or wind turbine in the case of a charging station with the DC bus configuration. The DC/AC converters can be used with PV in charging stations with the AC bus configuration.

The main contributions of this paper are:

- Design and control of a standalone DC FCS with two charging slots based on PV and battery energy storage.
- Study a real case for the proposed station in Alamein, Egypt.
- Sizing and power management of the charging station integrated into the PV/battery system takes into consideration various weather conditions and the EV load profile.
- Integrate a parallel resonant converter into the station instead of conventional DC/DC converters to maintain a constant current for charging and permit to use of a simple controller for fast charging algorithms.

## 2. SYSTEM DESCRIPTION

The proposed EV charging station is depicted in Fig. 1. It is a 100 kW standalone DC fast charging station powered by PV and battery energy storage. This station consists of two

charging slots, each with 50 kW maximum power. The charger consists of two modules of parallel resonant converter connected in parallel. PV is the main energy source for this station. However, as the PV output power is affected by the insolation level and environmental conditions, no power can be extracted from PV during the night. Battery energy storage (BES) is used to guarantee continuous electric power delivered to EVs. A DC/DC boost converter is used to integrate PV with the DC bus. Incremental conductance method (IC) is used as a maximum power point technique (MPPT) with the boost converter to extract maximum power from PV under various environmental conditions. A buck-boost converter is used between the DC bus and BES to control the charging and the discharging of BES.

TABLE 1 Specifications of the proposed station

Station maximum output power	100 kW
Number of Charging Slots	Two
Maximum Charging Current	120 A
Output Voltage	420 V
DC link Voltage	600 V

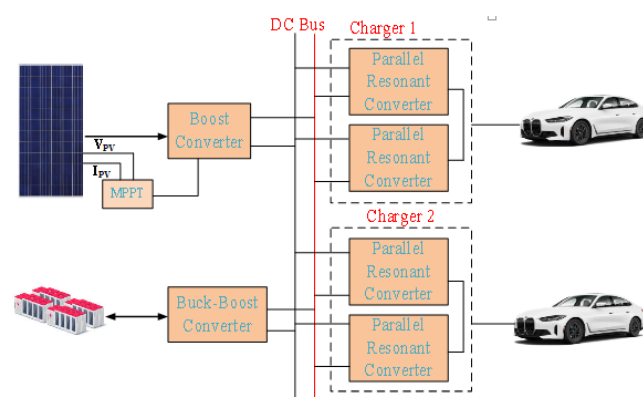


Fig. 1 Proposed DC fast charging station configuration  
EVs are connected to the DC bus through a parallel resonant converter. The specifications of the proposed station are shown in TABLE 1.

There are five modes of operation for the proposed station, as follows:

### Mode 1: PV to EV

If the PV power is equal to EV demand, then the EV will charge only from PV as shown in Fig. 2 (a).

### Mode 2: BES to EV

At night, When the power extracted from the PV equals zero, BES will deliver power to charge the EV as shown in Fig. 2 (b).

### Mode 3: PV and BES to EV

If the PV power is less than the EV demand, then BES will discharge to assist PV charging EVs as shown in Fig. 2 (c).

### Mode 4: PV to BES

If EV demand equals zero, then BES will store the power produced by PV as shown in Fig. 2 (d).

**Mode 5: PV to BES and EV**

If PV power is more than EV demand and the BES state of charge (SOC) is less than the maximum SOC, then the BES will store excess power as shown in Fig. 2 (e).

**3. Sizing of the proposed station**

The sizing of the proposed standalone station involves determining the power of the PV array and the battery storage capacity to meet the power requirement of the load at the designated location. This sizing depends on the weather conditions of the selected location such as the average solar irradiance.

**3.1.1 Solar radiation, temperature of selected Location.**

The location of the proposed EV charging station is the city of Alamein, Egypt (latitude 30° 49' N, longitude 28° 57' E). The solar radiation and temperature data are based on HOMER software [23]. The monthly average solar radiation is shown in **Error! Reference source not found..** The figure depicts that the solar radiation has maximum values in the summer months (7.83 kWh/m<sup>2</sup>/day in June 7.78 kWh/m<sup>2</sup>/day in July and 7.2 kWh/m<sup>2</sup>/day in August). The annual average solar radiation is 5.44 kWh/m<sup>2</sup>/day. Fig. 4 depicts the average temperature per month. The annual average temperature is 20.23 °C.

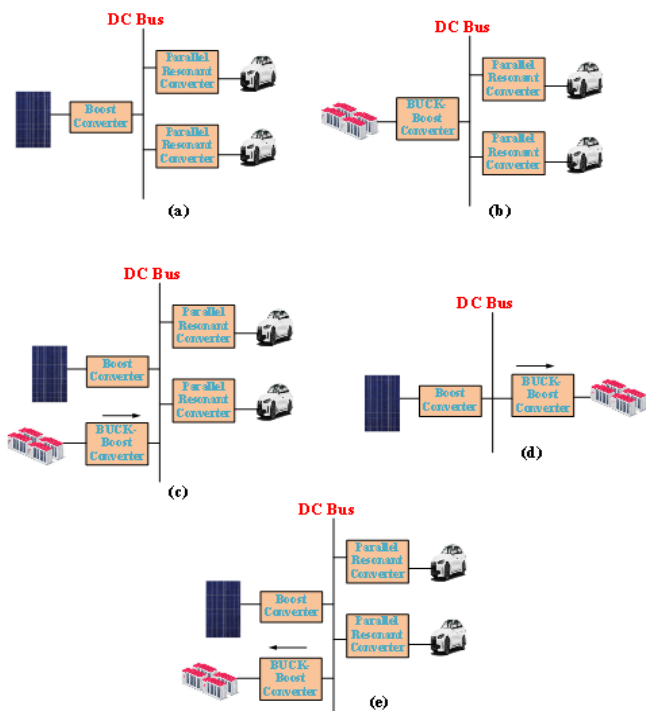


**Fig. 2** Modes of Operations. (a) Mode1: PV to EV; (b) Mode2: BES to EV; (c) Mode3: PV and BES to EV; (d) Mode (4): PV to BES; (e) Mode5: PV to BES and EV.

**3.1.2 Load Profile**

The daily and monthly load profiles are shown in Fig. 5. The load profile is based on the following: The number of

charging slots is two, the maximum power per charger is 50 kW, the average number of sessions per day is 15, vehicles can queue if all chargers are used, Vehicles arrive at the station with 20% SOC and the maximum SOC reached by vehicle charging is 80%, the average recharging time is 30 minutes, 80% of vehicles arrive at the station with a battery capacity of 50 kWh, and the remaining 20% of vehicles have a battery capacity of 150 kWh. Based on the above assumptions, the peak load power is 100 kW and the average load per day is 558 kWh/day.

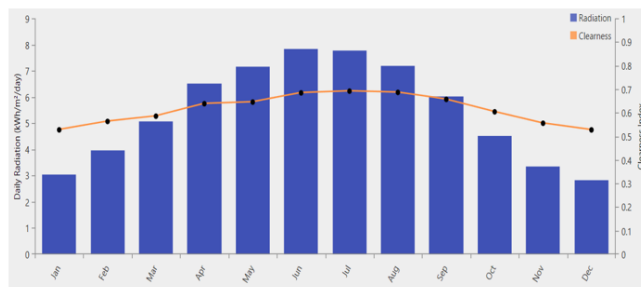


**Fig. 3** Average solar radiation per month

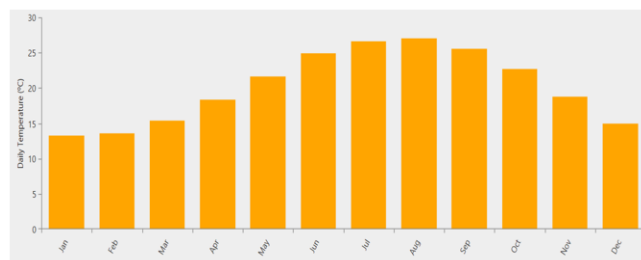


**Fig. 4** Average temperature per month

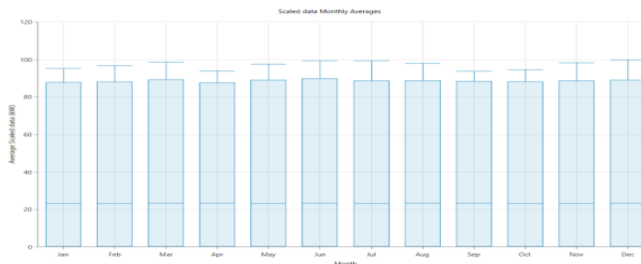
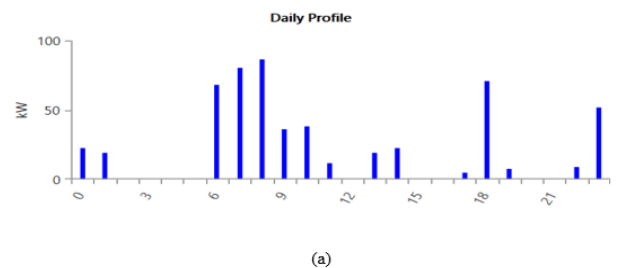


**Fig. 5** Load profile: (a) daily load profile, (b) monthly load profile

**3.2 PV and battery storage design**

The power generated by the PV is obtained as

$$P_{PV} = Y_{PV} f_{PV} \left( \frac{G_T}{G_{T,STC}} \right) [1 + \alpha_p (T_c - T_{c,STC})] \quad (1)$$

Where  $Y_{PV}$  is the rated capacity of the PV array under [standard test conditions](#)(kW),  $f_{PV}$  is the [PV derating factor](#) [%],  $G_T$  is the [solar radiation incident on the PV array](#) [kW/m2],  $G_{T,STC}$  is the incident radiation at [standard test conditions](#) [1 kW/m2],  $\alpha_p$  is the [temperature coefficient of power](#) [%/°C],  $T_c$  is the [PV cell temperature](#)[°C],  $T_{c,STC}$  is the PV cell temperature under [standard test conditions](#) [25°C].

The specifications of the PV module used in the design are shown in TABLE 2 [24].

TABLE 2 Specification of PV module

Manufacture	Canadian Solar
Maximum Power ( $P_{Max}$ )	330 W
Maximum Power Voltage ( $V_{MP}$ )	37.2 V
Maximum Power Current ( $I_{MP}$ )	8.88 A
Open Circuit Voltage ( $V_{OC}$ )	45.6 V
Short Circuit Current ( $I_{SC}$ )	9.45 A

The battery storage capacity can be calculated from the following formula.

$$C_{kWh} = (E_L \times AD) / (DoD \times \eta_{BS}) \quad (2)$$

Where  $E_L$  is the average load demand (kWh/d),  $AD$  are days of autonomy (h), DoD is depth of discharge,  $\eta_{BS}$  is battery storage efficiency.

The specifications of the battery storage module used in the design are shown in

TABLE 3 [25].

TABLE 3 Battery storage module specifications

Manufacture	TROJAN
Model	SOLAR SAGM 12 105
Type	Lead Acid
Voltage	12V
Capacity	105Ah@20Hr
Internal Resistance	4.8mΩ

TABLE 4 HOMER simulation results

PV Power (kW)	165
Batteries kWh	4456.25
Energy Production(kWh/yr.)	293.79
Energy consumption(kWh/yr.)	203.588
Excess Energy (kWh/yr.)	70.478(24%)
nmet Load (kWh/yr.)	81.5(0.04%)
Autonomy(hr.)	115
Battery Depth of Discharge	60%

Based on the average load demand of the day, the location of the proposed station and the specification of battery storage the HOMER results which satisfy the system requirements with economical cost are shown in

TABLE 4.

The number of PV modules in series can be determined as

$$\text{Number of modules in series} = \frac{\text{PV Array Voltage}}{\text{Module Voltage } (V_{MP})} \quad (3)$$

In this work, the PV array voltage is selected to be 400 V. Based on the PV array voltage, 11 PV modules are connected in series.

The number of PV modules in parallel can be determined as

$$\text{Number of modules in parallel} = \frac{\text{PV Array Current}}{\text{Module Current } (I_{MP})} = 47 \text{ modules} \quad (4)$$

The number of PV modules= 11 \* 47 =517 modules

For battery storage, the number of batteries in series

$$\text{Number of Batteries in series} = \frac{\text{Battery Bank Voltage}}{\text{Voltage of Battery module}} \quad (5)$$

In this work, the battery bank voltage is selected to be 300 V. Based on the battery bank voltage, 25 batteries are connected in series.

The number of batteries in parallel

$$\text{Number of Batteries in parallel} = \frac{\text{Battery storage rating (Ah)}}{\text{Capacity of battery}} = 142 \text{ batteries} \quad (6)$$

the total number of batteries= 25 \*142= 3550 batteries

HOMER program draws the output of each system part. For example, the power production from PV over a year is depicted in Fig. 7 The figure shows that the maximum power extracted from PV is 163 kW. With respect to the battery bank, the charging and discharging power in one year are shown in Fig. 7 and Fig. 8. The energy input to the battery is 137.253 MWh/year. The energy output from the battery bank is 117.53 MWh/year. Fig. 9 depicts the state of charge of the battery bank over the year. The minimum SOC of the battery bank is 40.85% in December. Whereas SOC is over 90% in the summer season.

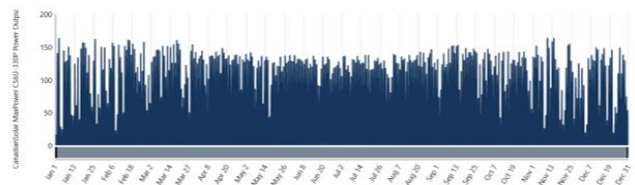


Fig. 6 PV output power

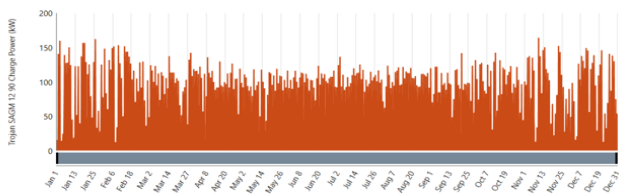


Fig. 7 Battery bank charging power

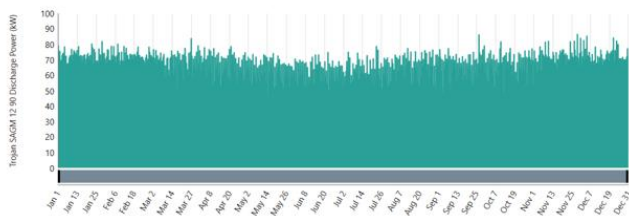


Fig. 8 Battery bank discharge power

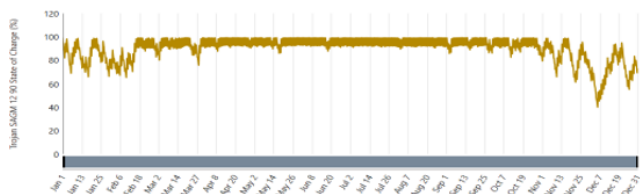


Fig. 9 Battery bank state of charge

### 3.3 Converters Design

#### 3.3.1 Boost converter design

The structure of the converter consists of a DC voltage source which is the voltage of the PV array, energy storage elements such as inductor and capacitor, diode, and semiconductor switch. The Boost converter is used between the PV and the DC bus to match the PV voltage to the DC bus voltage. The parameters of boost converters are indicated in TABLE 5.

TABLE 5 Boost converter parameters.

PV voltage ( $V_{PV}$ )	400 V
DC link voltage ( $V_{DC-Link}$ )	600 V
Switching Frequency ( $F_s$ )	10 kHz
Inductance ( $L$ )	300 $\mu$ H
Input Capacitance ( $C_{IN}$ )	200 $\mu$ F
Output Capacitance ( $C_{OUT}$ )	5000 $\mu$ F

#### 3.3.2 Buck-Boost Converter Design

The buck-boost converter is a bidirectional converter that can operate in two quadrants. It consists of two MOSFET switches ( $S_{BUCK}$ ,  $S_{BOOST}$ ). The first switch ( $S_{Buck}$ ) is used to control the charging process of the battery bank. The second switch ( $S_{Boost}$ ) controls the discharge process. An inductor ( $L$ ) that is responsible for transferring energy between the two sides of the converter. Two capacitors ( $C_{Buck}$ ,  $C_{Boost}$ ) which

are used to smooth the DC voltage at both sides of the converter.

The parameters of the buck-boost converters are indicated in TABLE 6.

TABLE 6 Parameters of buck-boost converter.

PV voltage ( $V_{PV}$ )	400 V
DC link voltage ( $V_{DC-Link}$ )	600 V
Switching Frequency ( $F_s$ )	10 kHz
Inductance ( $L$ )	320 $\mu$ H
Buck Capacitance ( $C_{Buck}$ )	5000 $\mu$ F
Output Capacitance ( $C_{Boost}$ )	2000 $\mu$ F

#### 3.3.3 Parallel resonant converter

The parallel resonant converter has many advantages, such as reducing ripples at the output current, providing no-load regulation, and protection against short circuit conditions. As shown in **Error! Reference source not found.**, the structure of the converter consists of a DC voltage source and a full bridge inverter that converts DC voltage to AC square wave. This voltage is applied to the resonant circuit ( $L_r$ ,  $C_r$ ). The voltage across the resonant capacitor voltage is rectified and filtered by ( $L_f$ ,  $C_f$ ).

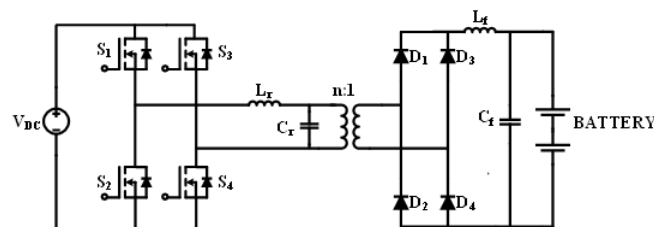


Fig. 10 Parallel resonant converter

The parameters of the parallel resonant converter are indicated in TABLE 7.

TABLE 7 Parameters of parallel resonance converter.

Switching frequency ( $F_{sw}$ )	10 kHz
Transformer turns ratio(n)	10/7
Resonant inductor ( $L_r$ )	220.26 $\mu$ H
Resonant capacitor ( $C_r$ )	1.15 $\mu$ F
Filter inductor ( $L_f$ )	1 mH
Filter capacitor ( $C_f$ )	100 $\mu$ F
Input DC voltage ( $V_{DC}$ )	600 V
Output DC voltage ( $V_o$ )	420 V

### 4. System control

The control of the proposed system is shown in Fig. 11 and

Fig. 12. The maximum power point tracking (MPPT) algorithm is used to extract maximum power from PV and then adjusts the duty cycle of the boost converter to achieve MPPT. The buck-boost controller is used to regulate the DC link voltage. The controller of the parallel resonant converter is used to control the current and voltage of the EV battery.

**4.1 MPPT controller**

MPPT techniques are used to extract maximum power from PV under various loads and environmental conditions. MPPT techniques are classified into two main categories [26]. The first category is conventional techniques such as Perturb and Observe method (P&O) and incremental conductance method (IC). The second category is artificial intelligence techniques such as artificial neural network method and fuzzy logic control method. The Incremental conductance method is discussed in this work due to its simplicity.

**4.2 Bidirectional buck-boost converter control.**

The objective of bidirectional buck-boost converter control is to regulate the DC link voltage. The control block diagram is shown in Fig. 11. A negative feedback signal of the DC link voltage is compared to the desired reference value to extract the error signal. The error signal is processed by the PI controller (PI1) to provide the value of the battery storage reference current (IB-ref) then, (IB-ref) is compared to the battery storage measured current (IB) and the error produced is processed by the PI controller (PI2) to produce the duty cycle for converter switches. The PI controllers’ gains of the DC link controllers are obtained using the Particle Swarm Optimization (PSO) optimization technique.

$$I_{B-ref} = (V_{DC-ref} - V_{DC}) (K_{p1} + \frac{K_{i1}}{S}) \quad (7)$$

$$D(\text{Duty cycle}) = (I_B - I_{B-ref}) (K_{p2} + \frac{K_{i2}}{S}) \quad (8)$$

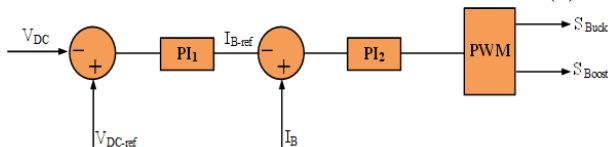


Fig. 11 Bidirectional buck-boost converter control

**4.3 Parallel resonant converter control**

constant current constant voltage (CCCV) method is considered one of the charging methods of electric vehicle batteries. In the constant current (CC) mode the battery charges with constant current and the battery voltage increases until it reaches a pre-set maximum value and then

the converter switches from CC mode to CV mode. In CV mode the battery voltage is constant whereas the battery charging current gradually decreases. As the parallel resonant converter acts as a current source when it operates at the resonance frequency, there is no need for the controller at CC charging mode and the converter can operate in open loop. As shown in Fig. 12, at CV mode, duty ratio control is implemented using a PI controller [27].

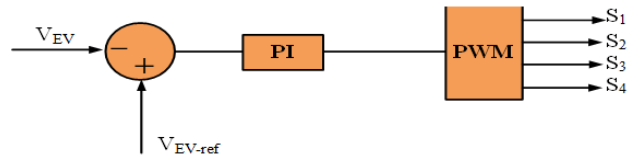


Fig. 12 Parallel resonant converter control

**5. Simulation Results and Discussion**

To verify the performance of the proposed system, two different case studies are simulated. The data of the weather conditions of the first case study are taken on a summer day (3 August). The data of the weather conditions of the second case study are taken on a winter day (2 January).

**5.1 First case study (3 August)**

The variation of solar radiation and PV cell temperature according to data taken from HOMER are shown in Fig. 13. The maximum radiation is 800 W/m<sup>2</sup> at 12 p.m., while the PV cell temperature varies from 27.01 °C to 47.38 °C. The voltage of the DC bus at various load conditions is depicted in Fig. 14. The figure shows that the DC bus voltage is 600V with a maximum voltage ripple of 7V (1.16%) The output power of PV, battery bank, and the load power demand are shown in Fig. 15. From 12 a.m. to 1 a.m., the battery storage delivers power to the load. From 2 a.m. to 5 a.m., the load demand is zero and no power is produced from the PV. The figure also shows that from 6 a.m. to 8 a.m., the load power demand is greater than PV power, so PV and battery bank share feeding the load. From 9 a.m. to 5 p.m., the PV power is greater than the load demand, so the battery bank stores the excess power. During the night, battery storage delivers power to the load. The state of charge of the battery bank is shown in Fig. 16. The figure shows that the battery bank charges and discharges according to the PV available power.

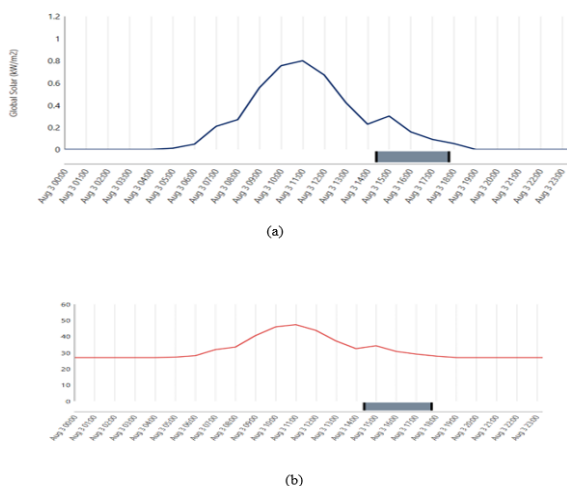


Fig. 13 Atmospheric condition of the case study (1): (a) solar radiation, (b) PV cell temperature

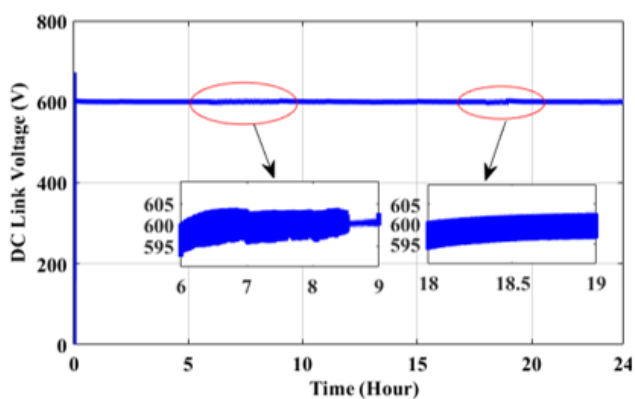


Fig. 14 DC link Voltage of case study (1)

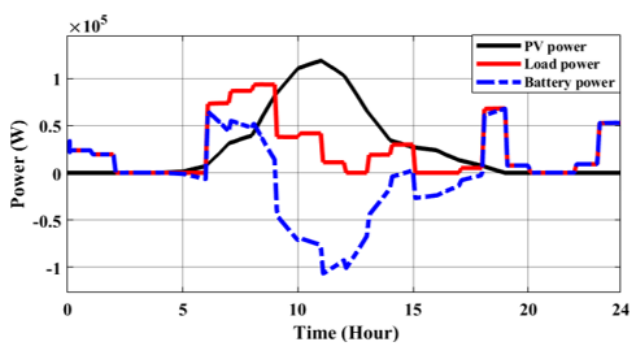


Fig. 15 Output power of case study (1)

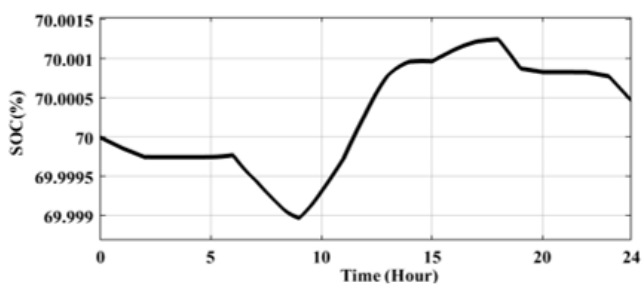


Fig. 16 Battery storage state of charge for case (1)

5.2 Second case study (2 January)

Fig. 17 shows the variation of solar radiation and PV cell temperature according to data taken from HOMER. The figure depicts that the maximum radiation is 110 W/m<sup>2</sup> at 9 a.m., while the PV cell temperature varies from 13.28 °C to 15.97 °C.

Fig. 18 depicts the voltage of the DC bus at various load conditions. The figure shows that the DC bus voltage is 600V with a maximum voltage ripple of 7V.

The output power of the system is shown in Fig. 19. The figure shows that the power produced by the PV is very low due to the low value of solar irradiance and the battery storage delivers power to the load for most hours of the day.

The state of charge of battery storage is shown in Fig. 20. The figure depicts that the battery storage discharges most of the day.

6. CONCLUSION

This paper presents the design and control of a standalone 100 kW DC fast charging station with two charging slots for electric vehicles. The station is based on photovoltaic as a primary energy source and battery energy storage. The proposed station is designed for a real location in Alamein Egypt using HOMER software. The station control is discussed. The performance of the proposed station at different solar irradiance and temperature is verified using MATLAB Simulink. The simulation results show that the voltage of the DC bus is stable with a maximum ripple voltage of 7V (1.16%) under various loads and the power of PV and battery storage can meet the various load conditions. In future work, the energy management of the proposed station will be investigated in the case of grid-connected and vehicle-to-grid (V2G)

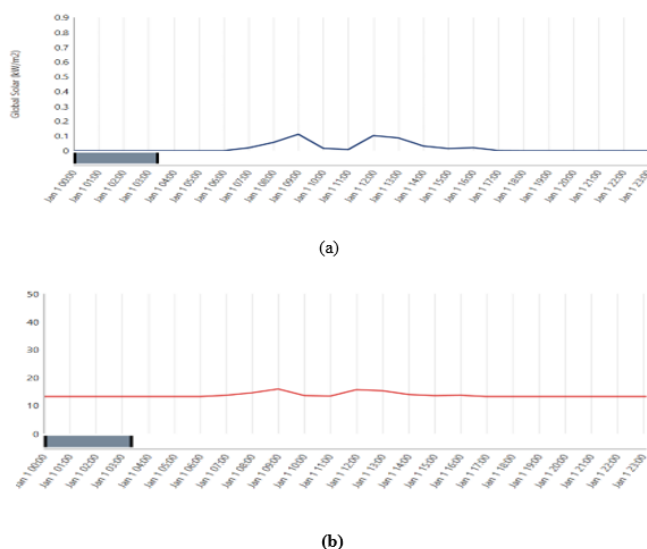


Fig. 17 Atmospheric condition of case study (2): (a) solar radiation, (b) PV cell temperature

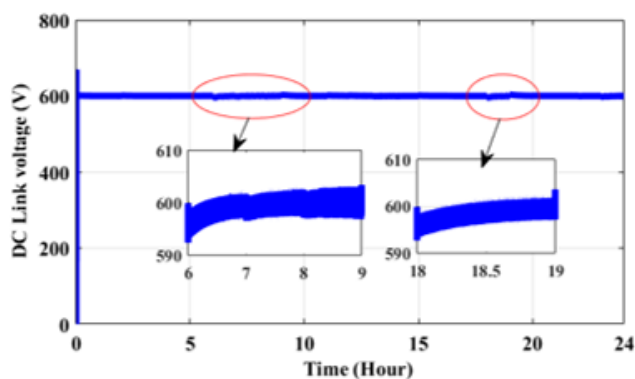


Fig. 18 DC link voltage of case (2)

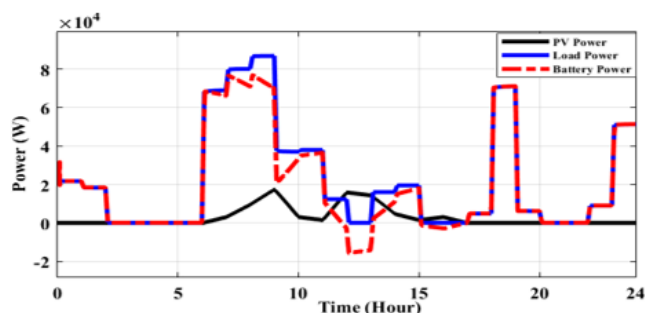


Fig. 19 Output power of case study (2)

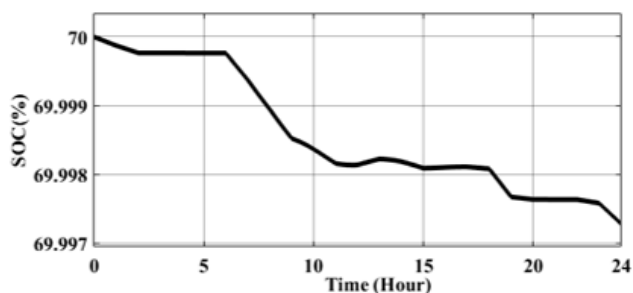


Fig. 20 Battery storage state of charge for case (2)

## References

- [1] K. Dimitriadou, N. Rigogiannis, S. Fountoukidis, F. Kotarela, A. Kyritsis, and N. Papanikolaou, "Current Trends in Electric Vehicle Charging Infrastructure; Opportunities and Challenges in Wireless Charging Integration," *Energies*, vol. 16, no. 4, p. 2057, Feb. 2023, doi: 10.3390/en16042057.
- [2] Metais, M. O., Jouini, O., Perez, Y., Berrada, J., & Suomalainen, E., "Too much or not enough? Planning electric vehicle charging infrastructure: A review of modeling options", *Renewable and Sustainable Energy Reviews*, 153, 111719, 2022.
- [3] Sajjad, A., Asmi, F., Chu, J. et al. "Environmental concerns and switching toward electric vehicles: geographic and institutional perspectives", *Environmental Science and Pollution Research*, 27, 39774–39785, 2020. <https://doi.org/10.1007/s11356-020-08311-4H>.
- [4] Tu, H. Feng, S. Srdic and S. Lukic, "Extreme Fast Charging of Electric Vehicles: A Technology Overview," in *IEEE Transactions on Transportation Electrification*, vol. 5, no. 4, pp. 861-878, Dec. 2019, doi: 10.1109/TTE.2019.2958709.
- [5] M. A. H. Rafi and J. Bauman, "A Comprehensive Review of DC Fast-Charging Stations with Energy Storage: Architectures, Power Converters, and Analysis," in *IEEE Transactions on Transportation Electrification*, vol. 7, no. 2, pp. 345-368, June 2021, doi: 10.1109/TTE.2020.3015743.
- [6] L. Wang, Z. Qin, T. Slangen, P. Bauer and T. van Wijk, "Grid Impact of Electric Vehicle Fast Charging Stations: Trends, Standards, Issues and Mitigation Measures - An Overview," in *IEEE Open Journal of Power Electronics*, vol. 2, pp. 56-74, 2021, doi: 10.1109/OJPEL.2021.3054601.
- [7] Ahmad, Fareed, Atif Iqbal, Imtiaz Ashraf, and Mousa Marzband. "Optimal location of electric vehicle charging station and its impact on distribution network: A review.", *Energy Reports* 8, 2022, 2314-2333.
- [8] Srivastava, A., Manas, M., & Dubey, R. K. "Electric vehicle integration's impacts on power quality in distribution network and associated mitigation measures: a review", *Journal of Engineering and Applied Science*, 70(1), 1-29, 2023.
- [9] A. Hussain, V.-H. Bui, J.-W. Baek, and H.-M. Kim, "Stationary Energy Storage System for Fast EV Charging Stations: Simultaneous Sizing of Battery and Converter," *Energies*, vol. 12, no. 23, p. 4516, Nov. 2019, doi: 10.3390/en12234516.
- [10] H. Polat *et al.*, "A Review of DC Fast Chargers with BESS for Electric Vehicles: Topology, Battery, Reliability Oriented Control and Cooling Perspectives," *Batteries*, vol. 9, no. 2, p. 121, Feb. 2023, doi: 10.3390/batteries9020121.
- [11] G. Alkaws, Y. Baashar, D. Abbas U, A. A. Alkahtani, and S. K. Tiong, "Review of Renewable Energy-Based Charging Infrastructure for Electric Vehicles," *Applied Sciences*, vol. 11, no. 9, p. 3847, Apr. 2021, doi: 10.3390/app11093847.
- [12] G. Rituraj, G. R. C. Mouli, and P. Bauer, "A Comprehensive Review on Off-Grid and Hybrid Charging Systems for Electric Vehicles," in *IEEE Open Journal of the Industrial Electronics Society*, vol. 3, pp. 203-222, 2022, doi: 10.1109/OJIES.2022.3167948.
- [13] A. Ali *et al.*, "Latest Energy Storage Trends in Multi-Energy Standalone Electric Vehicle Charging Stations: A Comprehensive Study," *Energies*, vol. 15, no. 13, p. 4727, Jun. 2022, doi: 10.3390/en15134727.
- [14] Awad, Mohamed, Ahmed M. Ibrahim, Zuhair Muhammed Alaas, Adel El-Shahat, and Ahmed I. Omar. "Design and analysis of an efficient photovoltaic energy-powered electric vehicle charging station using perturb and observe MPPT algorithm.", *frontiers in energy research* 10, 2022, 969482.
- [15] Ekren, Orhan, Celal Hakan Canbaz, and Çetin Berk Güvel. "Sizing of a solar-wind hybrid electric vehicle charging station by using HOMER software.", *Journal of Cleaner Production* 279, 2021, 123615.
- [16] I. E. Atawi, E. Hendawi, and S. A. Zaid, "Analysis and Design of a Standalone Electric Vehicle Charging Station Supplied by Photovoltaic Energy," *Processes*, vol. 9, no. 7, p. 1246,

- Jul. 2021, doi: 10.3390/pr9071246.
- [17] Iannuzzi, Diego, and Pasquale Franzese. "Ultrafast charging station for electrical vehicles: Dynamic modelling, design and control strategy.", *Mathematics and Computers in simulation* 184, 2021, 225-243.
- [18] A. Haque, V. S. B. Kurukuru and M. Ali Khan, "Energy Management Strategy for Grid Connected Solar Powered Electric Vehicle Charging Station," *2019 IEEE Transportation Electrification Conference (ITEC-India)*, Bengaluru, India, 2019, pp. 1-6, doi: 10.1109/ITEC-India48457.2019.ITECINDIA2019-44.
- [19] Q. Dai, J. Liu, and Q. Wei, "Optimal Photovoltaic/Battery Energy Storage/Electric Vehicle Charging Station Design Based on Multi-Agent Particle Swarm Optimization Algorithm," *Sustainability*, vol. 11, no. 7, p. 1973, Apr. 2019, doi: 10.3390/su1107197
- [20] Bassa de los Mozos, Albert, Gautham Ram Chandra Mouli, and Pavol Bauer. "Evaluation of topologies for a solar powered bidirectional electric vehicle charger.", *IET Power Electronics* 12, no. 14, 2019, 3675-3687.
- [21] He, Fulin, and Hassan Fathabadi. "Novel standalone plug-in hybrid electric vehicle charging station fed by solar energy in presence of a fuel cell system used as supporting power source.", *Renewable Energy* 156, 2020, 964-974.
- [22] Prem, P., P. Sivaraman, J. S. Sakthi Suriya Raj, M. Jagabar Sathik, and Dhafer Almakhlis. "Fast charging converter and control algorithm for solar PV battery and electrical grid integrated electric vehicle charging station.", *Automatika* 61, no. 4, 2020, 614-625.
- [23] <https://www.homerenergy.com/products/index.html>
- [24] C. Solar Inc, "Canadian Solar - CS6U-P MaxPower Datasheet." [Online]. Available: [www.canadiansolar.com/na](http://www.canadiansolar.com/na). (accessed 27 August 2023)
- [25] <https://www.trojanbattery.com/products/solar-saes-12-205-12v-aes-battery>. (accessed 27 August 2023)
- [26] A. I. M. Ali, Z. M. Alaas, M. A. Sayed, A. Almalaq, A. Farah, and M. A. Mohamed, "An Efficient MPPT Technique-Based Single-Stage Incremental Conductance for Integrated PV Systems Considering Flyback Central-Type PV Inverter," *Sustainability*, vol. 14, no. 19, p. 12105, Sep. 2022, doi: 10.3390/su141912105.
- [27] S. M. Ferdous, M. Asaduzzaman Shoeb, G. Shafiullah and M. A. Moin Oninda, "Parallel Resonant Converter for Battery Charging Application," *2019 9th International Conference on Power and Energy Systems (ICPES)*, Perth, WA, Australia, 2019, pp. 1-6, doi: 10.1109/ICPES47639.2019.9105578.